Electronic Supplementary Information

for

Enhanced power factor of n-type $Bi_2Te_{2.8}Se_{0.2}$ alloys through an efficient one-step sintering strategy for low-grade heat harvesting

Haoxiang Wei,[a] Jiaqi Tang,[a] Hongchao Wang[b] and Dongyan Xu*[a]

[a]*Department of Mechanical and Automation Engineering, The Chinese University of Hong Kong, Shatin, New Territories, Hong Kong Special Administrative Region, China. E-mail: dyxu@mae.cuhk.edu.hk*

[b]*School of Physics, State Key Laboratory of Crystal Materials, Shandong University, Jinan, China.*

I. Sintering temperature profiles

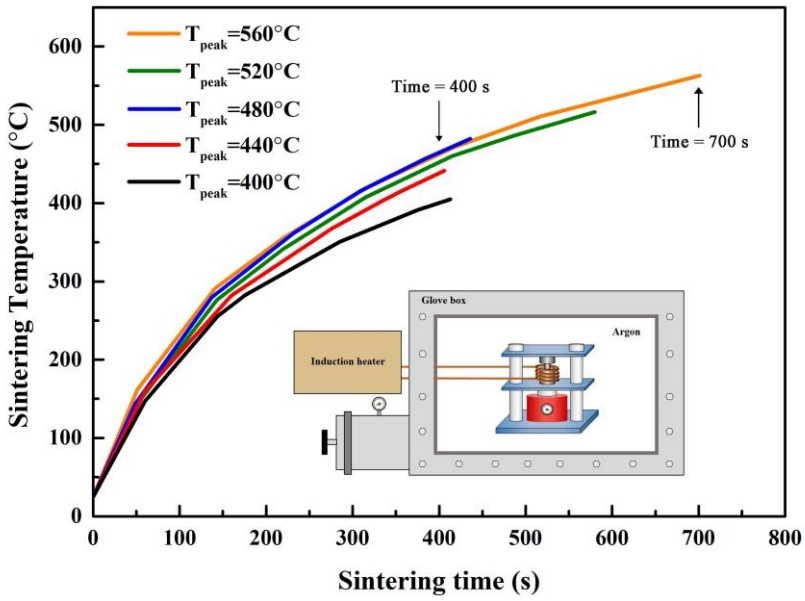

Fig. S1. Temporal sintering temperature profiles of the hot pressing processes. The inset shows the schematic of our home-made hot pressing system.

II. Lorenz number

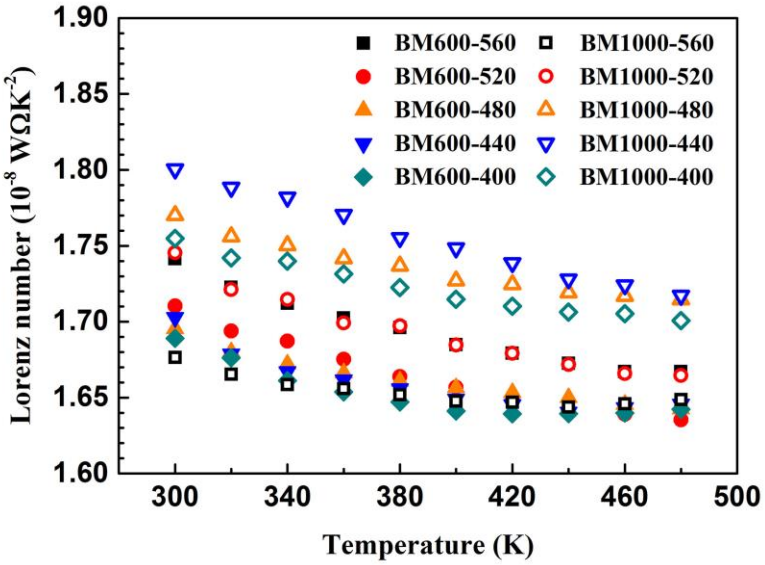

Fig. S2. Extracted Lorenz numbers of the sintered samples.

III. Repeatability of the power factor

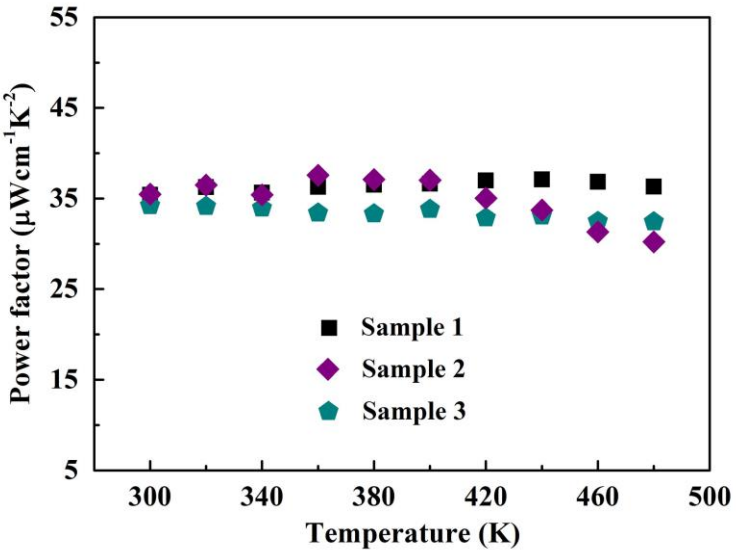

Fig. S3. Calculated power factors of three BM600-520 samples.

IV. Characterization of the TEG performance

Fig. S4 shows the schematic of the experimental setup for characterizing the TEG performance. An oxygen-free copper bar with the same cross-sectional area as the TEG was used as the heat flow meter. The temperature-dependent thermal conductivity of the oxygen-free copper was characterized in advance. There is a hole in the top part of the copper bar to accommodate a cartridge heater as a heat source. Four tiny holes with a diameter of 1 mm were drilled to the centerline of the copper bar for installing thermocouples. The copper bar was embedded in a thermal insulation block made of Teflon to reduce the heat loss to the surroundings. The cold side of the TEG was cooled by the open-loop water circulation.

Before testing, the TEG was connected with a potentiometer serving as an external load. The cartridge heater was turned on to provide heating to the hot side of the TEG. The heating power can be tuned by adjusting the heating current through the heater. When the system reached steady

state, the temperature distribution along the copper bar was measured using the installed thermocouples. According to Fourier's law, the heat input rate on the hot side of the TEG can be determined by

$$q = -k_{Cu} A \frac{dT}{dx} \tag{1}$$

where k_{Cu} is thermal conductivity of the oxygen-free copper, A is the cross-sectional area of the copper bar, and $\frac{dT}{dx}$ is the temperature gradient along the copper bar, which can be estimated through linearly fitting the temperature distribution measured by thermocouples. The voltage and current were recorded while adjusting the potentiometer over a suitable range. Under each temperature difference, the open-circuit voltage and the internal resistance of the TEG were obtained from the y-intercept and the slope of the V-I curve, respectively. The maximum output power was achieved when the external load matched the internal resistance of the TEG. The conversion efficiency of the TEG was calculated as the ratio of the maximum output power to the heat input rate by

$$\eta = \frac{P_{max}}{q} \tag{2}$$

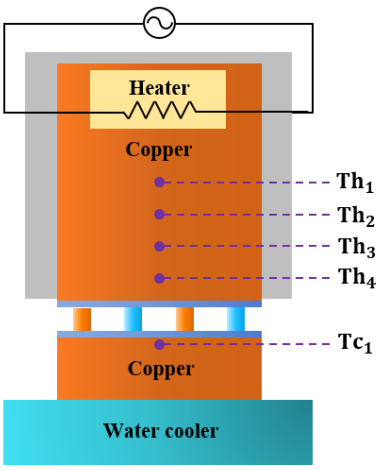

Fig. S4. Schematic of the experimental setup for characterizing the TEG performance.

V. Finite Element Modeling (FEM) of the TEG Performance

A FEM model was built in COMSOL based on the designed dimensions of TE pillars, electrodes, and substrates to analyze the effect of the contact thermal and electrical resistance on the performance of our TEG. The thickness of Ni electrodes was estimated to be 4 μm as seen in the SEM image in Fig. S5. The temperature-dependent thermoelectric properties of both n-type $Bi_2Te_{2.8}Se_{0.2}$ and p-type $Bi_{0.5}Sb_{1.5}Te_3$ alloys we experimentally determined were used in the FEM modelling.

Fig. S6(a) shows the device structure used in the FEM modelling and the temperature distribution in the TEG under ΔT = 128°C. The hot-side and cold-side temperatures were set according to the experimental conditions. The contact thermal and electrical resistance were extracted through fitting the experimental data and the results were shown in Fig. S6(c). The FEM results with the consideration of the contact resistance are also plotted in Fig. 10(a), which fit the experimental data very well. The ideal performance of our TEG under ΔT = 128°C was predicted by neglecting the contact thermal and electrical resistance in the FEM model and the results were shown in Fig. S6(d).

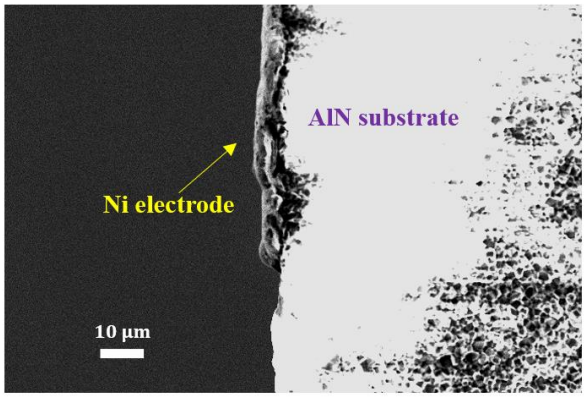

Fig. S5. SEM micrograph of the cross-section of the electroplated Ni electrode on the AlN substrate.

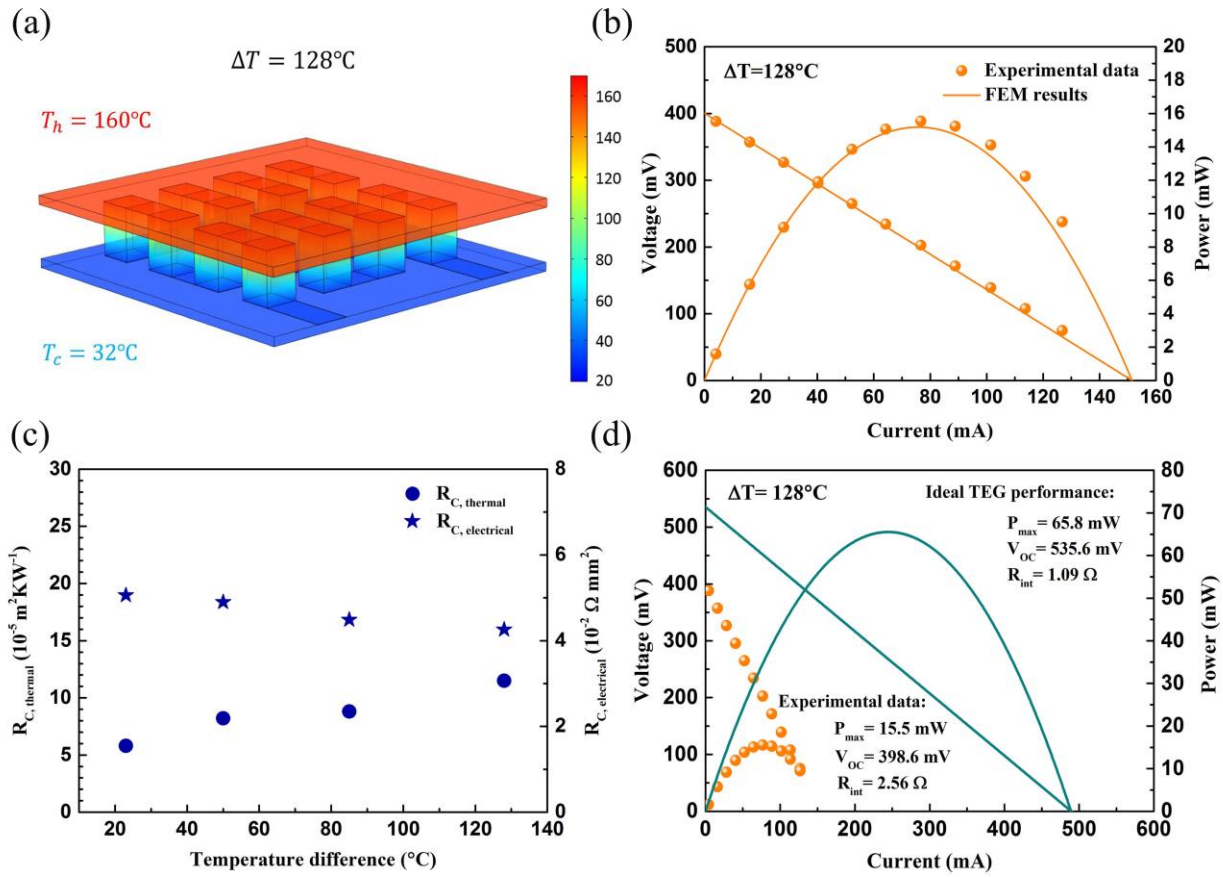

Fig. S6. (a) Device structure used in the FEM modelling and the temperature distribution in the TEG under ΔT = 128°C; (b) Experimental data and the FEM results with the consideration of the contact resistance under ΔT = 128°C; (c) Extracted contact thermal ($R_{C,\ thermal}$) and electrical resistance ($R_{C,\ electrical}$); (d) Ideal TEG performance under ΔT = 128°C if the contact resistance is completely eliminated.